

Crossed-beam reaction of carbon atoms with hydrocarbon molecules. V. Chemical dynamics of n -C₄H₃ formation from reaction of C(³P_{*j*}) with allene, H₂CCCH₂(X¹A₁)

R. I. Kaiser^{a)}

University of California, Department of Chemistry, Berkeley, California 94720, and Academia Sinica, Institute of Atomic and Molecular Sciences, 1, Section 4, Roosevelt Road, Taipei, 106, Taiwan, Republic of China, and Department of Physics, Technical University Chemnitz-Zwickau, 09107 Chemnitz, Germany

A. M. Mebel^{b)}

Academia Sinica, Institute of Atomic and Molecular Sciences, 1, Section 4, Roosevelt Road, Taipei, 106, Taiwan, Republic of China and Department of Chemistry, Tankang University, Tansui 25137, Taiwan, Republic of China

A. H. H. Chang^{c)} and S. H. Lin^{d)}

Academia Sinica, Institute of Atomic and Molecular Sciences, 1, Section 4, Roosevelt Road, Taipei, 106, Taiwan, Republic of China

Y. T. Lee^{e)}

University of California, Department of Chemistry, Berkeley, California 94720, and Academia Sinica, Institute of Atomic and Molecular Sciences, 1, Section 4, Roosevelt Road, Taipei, 106, Taiwan, Republic of China

(Received 15 December 1998; accepted 5 February 1999)

The crossed molecular beams technique was employed to investigate the reaction between ground state carbon atoms, C(³P_{*j*}), and allene, H₂CCCH₂(X¹A₁), at two averaged collision energies of 19.6 and 38.8 kJ mol⁻¹. Product angular distributions and time-of-flight spectra of C₄H₃ were recorded. Forward-convolution fitting of the data yields weakly polarized center-of-mass angular flux distributions isotropic at lower, but forward scattered with respect to the carbon beam at a higher collision energy. The maximum translational energy release and the angular distributions combined with *ab initio* and RRKM calculations are consistent with the formation of the n -C₄H₃ radical in its electronic ground state. The channel to the *i*-C₄H₃ isomer contributes less than 1.5%. Reaction dynamics inferred from the experimental data indicate that the carbon atom attacks the π -orbitals of the allenic carbon-carbon double bond barrierless via a loose, reactant-like transition state located at the centrifugal barrier. The initially formed cyclopropylidene derivative rotates in a plane almost perpendicular to the total angular momentum vector around its C-axis and undergoes ring opening to triplet butatriene. At higher collision energy, the butatriene complex decomposes within 0.6 ps via hydrogen emission to form the n -C₄H₃ isomer and atomic hydrogen through an exit transition state located 9.2 kJ mol⁻¹ above the products. The explicit identification of the n -C₄H₃ radical under single collision represents a further example of a carbon-hydrogen exchange in reactions of ground state carbon atoms with unsaturated hydrocarbons. This channel opens a barrierless route to synthesize extremely reactive hydrocarbon radicals in combustion processes, interstellar chemistry, and hydrocarbon-rich atmospheres of Jupiter, Saturn, Titan, as well as Triton.
© 1999 American Institute of Physics. [S0021-9606(99)01617-7]

I. INTRODUCTION

The chemical reactivity and formation of distinct structural isomers of hydrocarbon radicals is of major importance in combustion chemistry,¹ chemical processes in hydrocarbon-rich planetary atmospheres,² and outflow of dying carbon stars as well as interstellar clouds and hot molecular cores.³ In oxygen-deficit combustion flames, for example,

only *i/n*-C₄H₃ isomers are expected to play a crucial role in formation of the first aromatic ring, the phenyl radical C₆H₅, via the three body reaction i/n -C₄H₃+C₂H₂+M→C₆H₅+M. Here, M represents the third body collision partner, *i*- and *n*- the iso and normal C₄H₃ isomers, respectively.⁴ On the other hand, cyclic C₄H₃ isomers are expected not to form aromatic species. In addition, C₄H₃ isomers together with other hydrocarbon radicals are likely to be formed in extraterrestrial environments such as cold, molecular clouds and planetary atmospheres of Jupiter, Saturn, Uranus, and Neptune as well as the moons Titan and Triton.⁵ Recent support is based on the observation of the carbon-hydrogen exchange channel in crossed-beam reactions of atomic carbon C(³P_{*j*}) with unsaturated hydrocarbons, cf. reactions (1)–(5).⁶

^{a)}Author to whom correspondence should be addressed. Electronic mail: kaiser@po.iam.s.sinica.edu.tw

^{b)}Electronic mail: mebel@po.iam.s.sinica.edu.tw

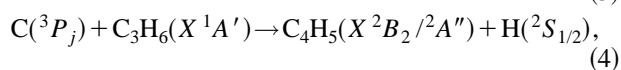
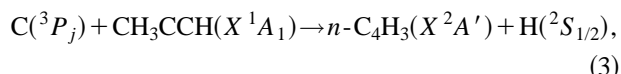
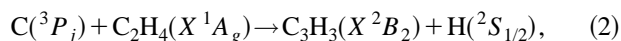
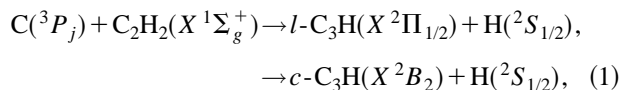
^{c)}Electronic mail: agnes@gate.sinica.edu.tw

^{d)}Electronic mail: hshaw@po.iam.s.sinica.edu.tw

^{e)}Electronic mail: ytle@gate.sinica.edu.tw

TABLE I. Experimental beam conditions and 1σ errors averaged over the experimental time: most probable velocity v_0 , speed ratio S , most probable relative collision energy, E_{coll} , center-of-mass angle, θ_{CM} , composition of the carbon beam, and flux factor $f_v = n(\text{C}) * n(\text{H}_2\text{CCCH}_2) * v_r$ in relative units, with the number density of the i th reactant n_i and the relative velocity v_r .

Beam	v_0 , ms^{-1}	S	E_{coll} , kJ mol^{-1}	θ_{CM}	$\text{C}_1:\text{C}_2:\text{C}_3$	f_v
$\text{C}(^3P_j)/\text{Ne}$	1894 ± 20	3.0 ± 0.2	19.6 ± 1.0	55.0 ± 0.6	1:0.7:0.8	1.0
$\text{C}(^3P_j)/\text{He}$	2784 ± 23	3.5 ± 0.3	38.8 ± 1.4	44.2 ± 0.6	1:0.2:0.85	1.5 ± 0.4
H_2CCCH_2	812 ± 10	8.2 ± 0.4	-	-	-	-



In this paper, we elucidate the intimate chemical dynamics of the atom-neutral reaction of $\text{C}(^3P_j)$ with a second C_3H_4 isomer, allene $\text{H}_2\text{CCCH}_2(X^1A_1)$ under single collision conditions at two collision energies of 19.6 kJ mol^{-1} and 38.8 kJ mol^{-1} . Our findings are compared with the reaction of $\text{C}(^3P_j)$ with methylacetylene, $\text{CH}_3\text{CCH}(X^1A_1)$ studied earlier. Energy-dependent, triply differential cross sections are derived from the experimental data and then combined with state-of-the-art *ab initio* and RRKM calculations to reveal unprecedented information on poorly explored triplet C_4H_4 and doublet C_4H_3 potential energy surfaces (PESs). These findings expose likely reaction pathways to hitherto unobserved extraterrestrial C_4H_3 isomer(s) and unravel potential synthetic routes to these radicals in combustion flame chemistry.

II. EXPERIMENTAL SETUP

The experiments were performed under single collision conditions using a universal crossed molecular beams apparatus described in Ref. 7 in detail. A pulsed supersonic carbon beam was generated via laser ablation of graphite at 266 nm.⁸ The 30 Hz, 40 mJ output of a Spectra Physics GCR-270-30 Nd:YAG laser was focused onto a rotating carbon rod, and the ablated carbon atoms were seeded into neon or helium released by a Proch-Trickl pulsed valve operating at 60 Hz, 80 μs pulses, and 4 atm backing pressure. A four-slot chopper wheel mounted 40 mm after the ablation zone selected a 9.0 μs segment of the seeded carbon beam. Table I summarizes the experimental beam conditions. The carbon beam and a pulsed allene beam hold at 660 ± 5 Torr backing pressure passed through skimmers and crossed at 90° in the interaction region of the scattering chamber. The reactively scattered products were detected in the plane defined by both beams using a rotatable detector consisting of a Brink-type electron-impact ionizer,⁹ quadrupole mass filter, and a Daly ion detector at laboratory angles in 2.5° and 5.0° steps between 10.0° and 60.0° with respect to the carbon beam. The

velocity distribution of the products was recorded using the time-of-flight (TOF) technique choosing a channel width of 7.5 μs . Information on the chemical dynamics of the reaction was gained by fitting the TOF spectra and the product angular distribution in the laboratory frame (LAB) using a forward-convolution routine.¹⁰ This approach initially assumes an angular flux distribution $T(\theta)$ and the translational energy flux distribution $P(E_T)$ in the center-of-mass system (CM). Laboratory TOF spectra and the laboratory angular distributions were then calculated from these $T(\theta)$ and $P(E_T)$ averaged over the apparatus and beam functions. Best TOF and laboratory angular distributions were archived by iteratively refining adjustable $T(\theta)$ and $P(E_T)$ parameters.

III. AB INITIO AND RRKM CALCULATIONS

The geometries of the reactants, products, various intermediates, and transition states for the $\text{C}(^3P_j) + \text{H}_2\text{CCCH}_2$ reaction were optimized using the hybrid density functional B3LYP method, i.e., Becke's three-parameter nonlocal exchange functional¹¹ with the nonlocal correlation functional of Lee, Yang, and Parr,¹² and the 6-311G(d,p) basis set.¹³ Vibrational frequencies, calculated at the B3LYP/6-311G(d,p) level, were used for characterization of stationary points, zero-point energy (ZPE) correction, and for the RRKM calculations. All the stationary points were positively identified for minimum (number of imaginary frequencies NIMAG=0) or transition state (NIMAG=1). In some cases, geometries and frequencies were recalculated at the MP2/6-311G(d,p) and CCSD(T)/6-311G(d,p) level.¹⁴

In order to obtain more reliable energies, we used the G2M(RCC,MP2)¹⁵ method, a modification of the Gaussian-2 [G2(MP2)] approach.¹⁶ The total energy in G2M(RCC,MP2) is calculated as follows:

$$E[\text{G2M(RCC,MP2)}]$$

$$= E[\text{RCCSD(T)/6-311G}(d,p)] + \Delta E(+3df2p)$$

$$+ \Delta E(\text{HLC}) + \text{ZPE}[\text{B3LYP/6-311G}(d,p)], \quad (6)$$

where

$$\Delta E(+3df2p)$$

$$= E[\text{MP2/6-311} + \text{G}(3df,2p)] - E[\text{MP2/6-311G}(d,p)] \quad (7)$$

and the empirical "higher level correction"

$$\Delta E(\text{HLC}) = -5.25n_\beta - 0.19n_\alpha, \quad (8)$$

where n_α and n_β are the numbers of α and β valence electrons, respectively. It has been shown that the

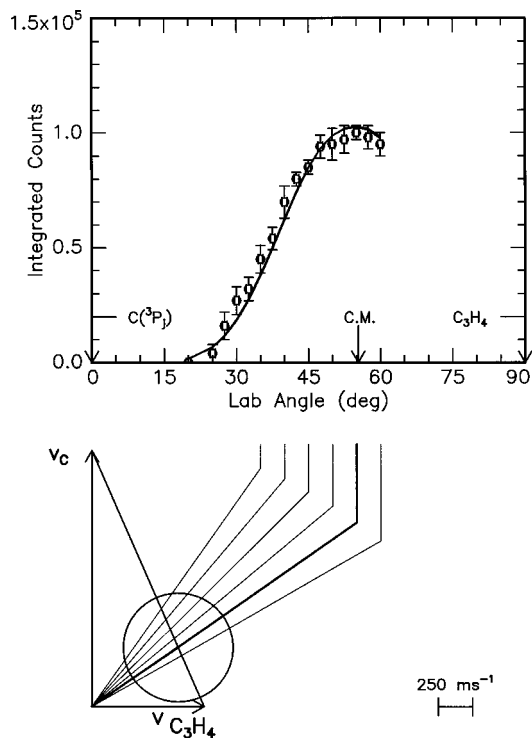


FIG. 1. Lower: Newton diagram for the reaction $C(^3P_j) + H_2CCCH_2(X^1A_1)$ at a collision energy of 19.6 kJ mol^{-1} . The circle stands for the maximum center-of-mass recoil velocity of the $n\text{-C}_4\text{H}_3$ isomer assuming no energy channels into the internal degrees of freedom. Upper: Laboratory angular distribution of product channel at $m/e=51$. Circles and 1σ error bars indicate experimental data, the solid lines the calculated distribution. C.M. designates the center-of-mass angle. The solid lines originating in the Newton diagram point to distinct laboratory angles whose TOFs are shown in Fig. 3.

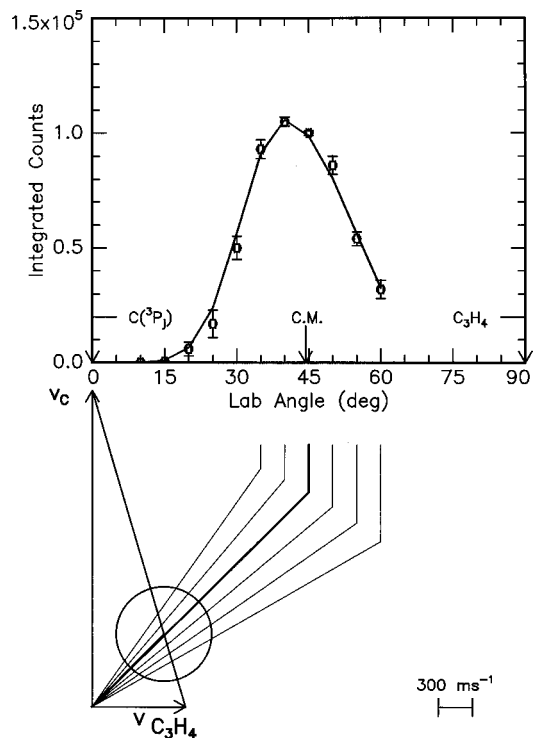


FIG. 2. Lower: Newton diagram for the reaction $C(^3P_j) + H_2CCCH_2(X^1A_1)$ at a collision energy of 38.8 kJ mol^{-1} . The circle stands for the maximum center-of-mass recoil velocity of the $n\text{-C}_4\text{H}_3$ isomer assuming no energy channels into the internal degrees of freedom. Upper: Laboratory angular distribution of product channel at $m/e=51$. Circles and 1σ error bars indicate experimental data, the solid lines the calculated distribution. C.M. designates the center-of-mass angle. The solid lines originating in the Newton diagram point to distinct laboratory angles whose TOFs are shown in Fig. 4.

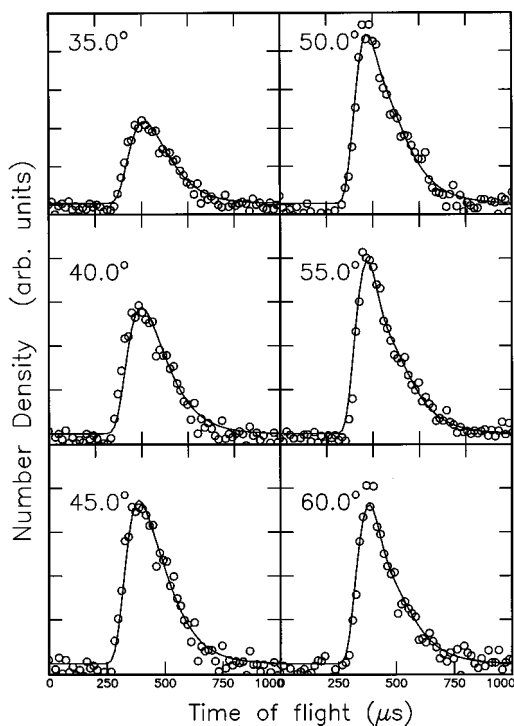


FIG. 3. Time-of-flight data at $m/e=51$ for indicated laboratory angles at a collision energy of 19.6 kJ mol^{-1} . Open circles represent experimental data, the solid line the fit. TOF spectra have been normalized to the relative intensity at each angle.

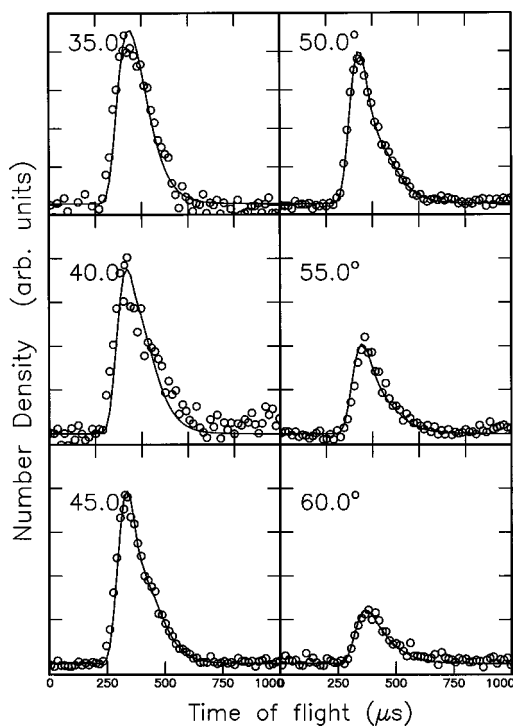


FIG. 4. Time-of-flight data at $m/e=51$ for indicated laboratory angles at a collision energy of 38.8 kJ mol^{-1} . Open circles represent experimental data, the solid line the fit. TOF spectra have been normalized to the relative intensity at each angle.

G2M(RCC,MP2) method gives the averaged absolute deviation of 4.8 kJ mol^{-1} of calculated atomization energies from experiment for 32 first-row G2 test compounds. The GAUSSIAN 94,¹⁷ MOLPRO 96,¹⁸ and ACES-II¹⁹ programs were employed for the potential energy surface computations. In this paper, we present only those results necessary to understand our experimental data. All details are given in a forthcoming publication.²⁰

According to the quasi-equilibrium theory or RRKM theory,²¹ rate constant $k(E)$ at a collision energy E for a unimolecular reaction $A^* \rightarrow A^\ddagger \rightarrow P$ can be expressed as

$$k(E) = \frac{\sigma}{h} \cdot \frac{W^\ddagger(E - E^\ddagger)}{\rho(E)}, \quad (9)$$

where σ is the symmetry factor, $W^\ddagger(E - E^\ddagger)$ denotes the total number of states of the transition state (activated complex) A^\ddagger with the barrier E^\ddagger , $\rho(E)$ represents the density of states of the energized reactant molecule A^* , and P is the product or products. The saddle point method²¹ was applied to evaluate $\rho(E)$ and $W(E)$. A simple scheme²² where the barrier along the reaction coordinate was assumed as an inverted parabola was applied to incorporate the tunneling corrections to the RRKM rate constants at the lower collision energy of 19.6 kJ mol^{-1} .

IV. RESULTS

A. Reactive scattering signal

Reactive scattering signal was observed at $m/e = 51$, i.e., C_4H_3 , cf. Figs. 1–4. TOF spectra were recorded at lower m/e values 50–48 as well but show identical TOF patterns. This finding indicates that the signal at these m/e ratios originates in cracking of the $C_4H_3^+$ parent in the ionizer and that channels 2–5 are absent under our experimental conditions, cf. Table II. In addition, no radiative associations to C_4H_4 ($m/e = 52$) could be detected, indicating that internally excited C_4H_4 collision complexes do not survive under single collision conditions employed in our experiments. Finally, no higher masses than $m/e = 51$ from reaction of C_2 and C_3 clusters were observed.

B. Laboratory angular distributions (LAB) and TOF spectra

The most probable Newton diagrams of the title reaction as well as the laboratory angular (LAB) distributions of the C_4H_3 product are displayed in Figs. 1 and 2 at collision energies of 19.6 and 38.8 kJ mol^{-1} , respectively. At lower collision energy, the LAB distribution peaks close to the CM

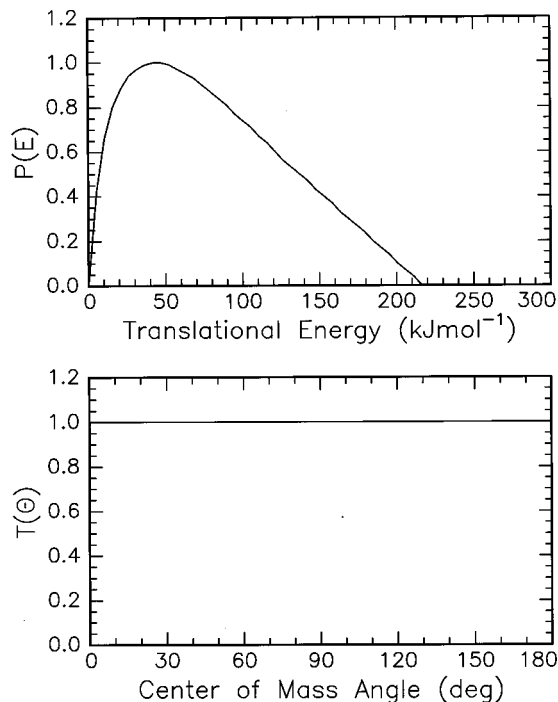


FIG. 5. Lower: Center-of-mass angular flux distributions for the reaction $C(^3P_j) + H_2CCCH_2(X^1A_1)$ at collision energies of 19.6 kJ mol^{-1} . Upper: Center-of-mass translational energies flux distributions for the reaction $C(^3P_j) + H_2CCCH_2(X^1A_1)$ at a collision energy of 19.6 kJ mol^{-1} . Dashed and solid lines limit the range of acceptable fits within 1σ error bars.

angle of 55.0° . As the collision energy rises, the LAB distribution shows a slightly forward peaking at 40.0° compared to the CM angle of 44.2° . This result hints to indirect reactive scattering dynamics through a long-lived C_4H_4 complex with a lifetime exceeding (19.6 kJ mol^{-1}) or comparable to its rotational period (38.8 kJ mol^{-1} , osculating complex). Further, both LAB distributions are very broad and extend to at least 50.0° in the scattering plane. This order-of-magnitude together with the $C_4H_3 + H$ product mass ratio of 51 points out that the averaged translational energy release $\langle E_T \rangle$ in the products is large and that the center-of-mass translational energy distributions $P(E_T)$'s peak away from zero, cf. Sec. IV C.

C. Center-of-mass translational energy distributions, $P(E_T)$

Figures 5 and 6 present the best fits of the translational energy distributions $P(E_T)$ and angular distributions $T(\theta)$ of the title reaction in the center-of-mass frame. The LAB distributions and TOF data were fitted with a single $P(E_T)$ extending to a maximum translational energy release E_{\max} of 215 kJ mol^{-1} and 240 kJ mol^{-1} at lower and higher collision energy, respectively. These high energy cutoffs are accurate within 25 kJ mol^{-1} . If the energetics of distinct isomers are well separated, E_{\max} can be used to identify individual C_4H_3 isomers. The maximal translational energy release, i.e., the sum of the reaction exothermicity and relative collision energy, suggests the formation of the n - C_4H_3 isomer. Here, the theoretical calculations expect high energy cutoffs of the $P(E_T)$'s of $E_{\max}(\text{theor.} = 19.6 \text{ kJ mol}^{-1}) = 199.5 \text{ kJ mol}^{-1}$ and

TABLE II. Thermochemistry of the reaction $C(^3P_j) + H_2CCCH_2(X^1A_1)$.

#	Exit channel	Reaction enthalpy at 0 K, $\Delta_R H(0 \text{ K}), \text{ kJ mol}^{-1}$
1	n - $C_4H_3(X^2A')$ + $H(^2S_{1/2})$	-179.9
2	$HCCCCH(X^1\Sigma_g^+) + H_2(X^1\Sigma_g^+)$	-450 ± 12
3	$HCCCCH(X^1\Sigma_g^+) + 2H(^2S_{1/2})$	-18 ± 5
4	$C_4H(X^2\Sigma) + H_2(X^1\Sigma_g^+) + H(^2S_{1/2})$	$+72 \pm 10$
5	$C_4(X^3\Sigma_g^-) + 2H_2(X^1\Sigma_g^+)$	$+62 \pm 15$

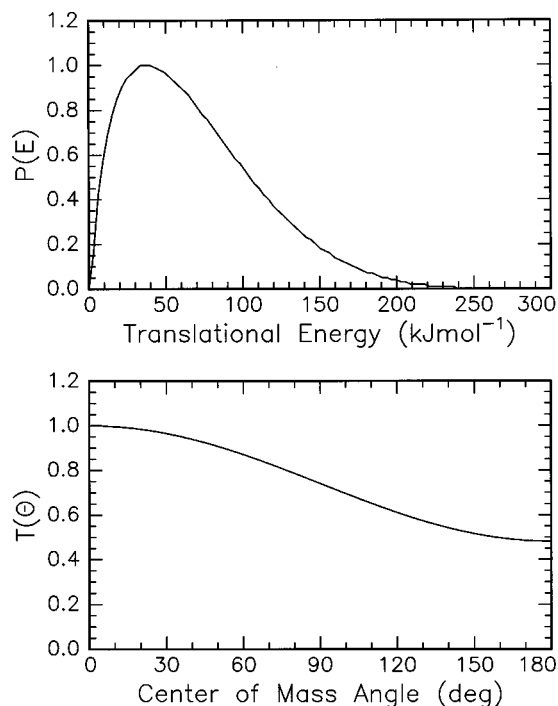


FIG. 6. Lower: Center-of-mass angular flux distributions for the reaction $C(^3P_j) + H_2CCCH_2(X^1A_1)$ at collision energies of 38.8 kJ mol^{-1} . Upper: Center-of-mass translational energies flux distributions for the reaction $C(^3P_j) + H_2CCCH_2(X^1A_1)$ at a collision energy of 38.8 kJ mol^{-1} . Dashed and solid lines limit the range of acceptable fits within 1σ error bars.

$E_{\text{max}}(\text{theor.} = 38.8 \text{ kJ mol}^{-1}) = 218.7 \text{ kJ mol}^{-1}$, are both in good agreement with our experimental data. The formation of the 46.9 kJ mol^{-1} less stable *i*- C_4H_5 can be excluded as a major contribution, since the maximum energy release is restricted to 153.9 and $173.1 \text{ kJ mol}^{-1}$ at higher and lower collision energy. However, minor contributions might prevail, cf. discussion in Sec. V. Furthermore, both $P(E_T)$'s peak away from zero as expected from the LAB distributions and depict a broad plateau between 30 and 50 kJ mol^{-1} . The fraction of energy channeling into translation of the products is quite large, i.e., 33 ± 3 and $30 \pm 2\%$ at higher and lower collision energy, respectively.

D. Center-of-mass angular distributions, $T(\theta)$

At lower collision energy, $T(\theta)$ is isotropic and symmetric around $\pi/2$, cf. Fig. 5. This implies that either the lifetime of the decomposing C_4H_4 complex is longer than its rotational period τ_r or that two hydrogen atoms of the C_4H_4 intermediate can be interconverted through a rotational axis.²³ In this case, the light H-atom could be emitted in θ and $\pi - \theta$ to result in the forward-backward symmetry of $T(\theta)$. However, as the collision energy rises, the center-of-mass angular distribution peaks forward with respect to the carbon beam (Fig. 6) suggesting a reduced lifetime of the fragmenting C_4H_4 complex as the collision energy rises (oscillating complex): A complex formation takes place, but the well depth along the reaction coordinate is too shallow to allow multiple rotations, and the complex decomposes with a random lifetime distribution before one full rotation elapses. Based on the intensity ratio of $T(\theta)$ at $\theta = 0^\circ$

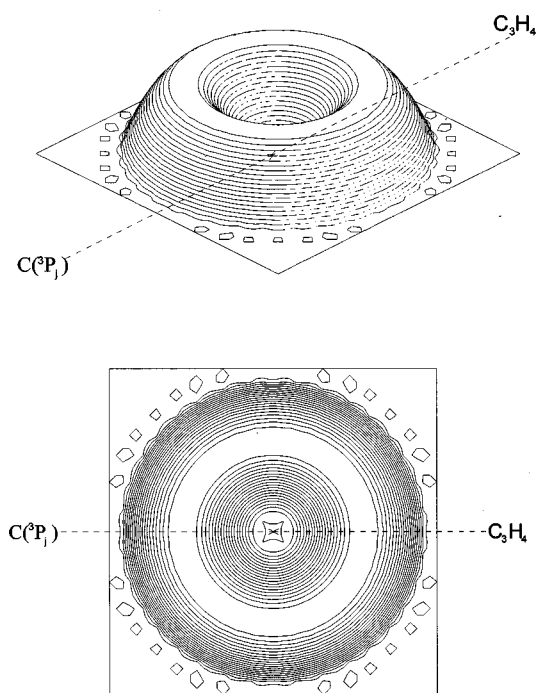


FIG. 7. Contour flux map for the reaction $C(^3P_j) + H_2CCCH_2(X^1A_1)$ at a collision energy of 19.6 kJ mol^{-1} . (a) Three-dimensional map; (b) two-dimensional projection.

and 180° of 2.1 ± 0.2 , the identification of the fragmenting complex enables us to use the rotational period of the complex as a molecular clock to estimate its lifetime (cf. Sec. V). To explain the forward peaking, the carbon atom and the leaving hydrogen atom must further be situated on opposite sites of the rotation axis of the fragmenting complex.⁵

The isotropic angular distribution at lower collision energy is the result of a poor coupling between the initial and final angular momentum vectors, \mathbf{L} and \mathbf{L}' , respectively, as already observed in crossed-beams reaction (2)–(5). If we calculate the maximum impact parameter b_{max} and the maximum orbital angular momentum L_{max} within the orbiting limit as outlined in Ref. 5 b_{max} yields $b_{\text{max}}(19.6 \text{ kJ mol}^{-1}) = 3.8 \text{ \AA}$, $b_{\text{max}}(38.8 \text{ kJ mol}^{-1}) = 3.2 \text{ \AA}$, $L_{\text{max}}(19.6 \text{ kJ mol}^{-1}) = 114\hbar$ and $L_{\text{max}}(38.8 \text{ kJ mol}^{-1}) = 132\hbar$. If we compare these numbers with the final orbital angular momentum L' as derived from acceptable *ab initio* exit impact parameters of decomposing triplet C_4H_4 isomers, cf. Sec. V, we find $L < 0.17L'$. Therefore, a large fraction of the initial orbital angular momentum is routed into rotational excitation of *n*- C_4H_3 .

E. Flux contour maps and total relative cross sections

Figures 7 and 8 depict the two and three dimensional center-of-mass flux contour plots $I(\theta, u) \sim P(u) * T(\theta)$ for collision energies at 19.6 and 38.8 kJ mol^{-1} . As expected from the center-of-mass angular distributions, data at lower collision energy show a forward-backward symmetric flux profile. As the collision energy rises, a forward peaking on

the relative velocity vector is obvious. Integrating this flux distribution and correcting for the reactant flux as well as relative reactant velocity (cf. Table I), we find an integrated relative reactive scattering cross section ratio of $\sigma(19.6 \text{ kJ mol}^{-1})/\sigma(38.8 \text{ kJ mol}^{-1}) = 1.9 \pm 0.6$ within our error limits, i.e., a rising cross section as the collision energy drops. This result together with recent bulk experiments²⁴ and our *ab initio* calculations, cf. Sec. V, suggest a barrierless, attractive long-range dispersion forces dominated reaction together with a loose, reactantlike entrance transition state located at the centrifugal barrier.⁵

V. DISCUSSION

In this section, we present the results of our *ab initio* calculations and feasible reaction pathways to distinct C_4H_3 isomers via insertion of the electrophile carbon atoms into the allenic C–H bond, addition to two π -molecular orbitals located either at two distinct carbon atoms or at the central carbon atom, and possible intersystem crossing (ISC) to the singlet surface (Sec. V A). The observed CM angular and translational energy distributions are then compared in Sec. V B to those distributions expected from possible reaction pathways elucidated from our *ab initio* calculations. We illustrate that large impact parameters dominate the reactive scattering dynamics. The reaction proceeds mainly via addition of $\text{C}(^3P_j)$ to the terminal carbon atoms of the allene molecule to a cyclopropylidene derivative C_4H_4 on the triplet surface. This intermediate ring opens to triplet butatriene,

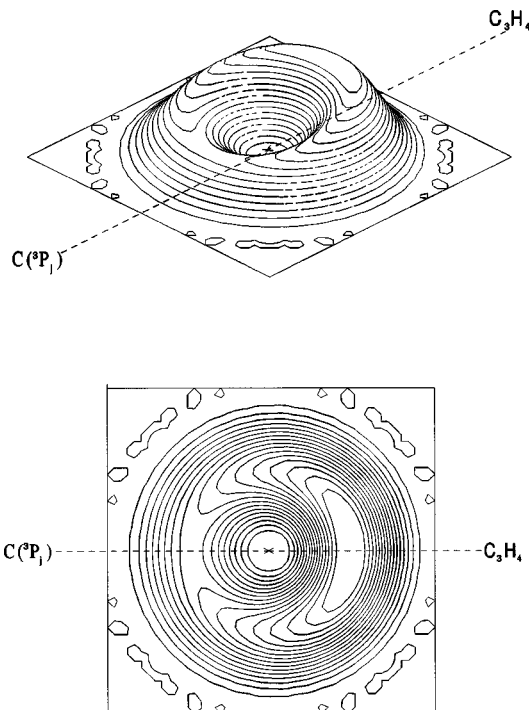


FIG. 8. Contour flux map for the reaction $\text{C}(^3P_j) + \text{H}_2\text{CCCH}_2(X^1A_1)$ at a collision energy of 38.8 kJ mol^{-1} . (a) Three-dimensional map; (b) two-dimensional projection.

which emits an H-atom to form the $n\text{-C}_4\text{H}_3$. As the collision energy rises, low impact parameter trajectories might add $\text{C}(^3P_j)$ to the central allenic carbon atom followed by ring closure to the cyclopropylidene derivative C_4H_4 .

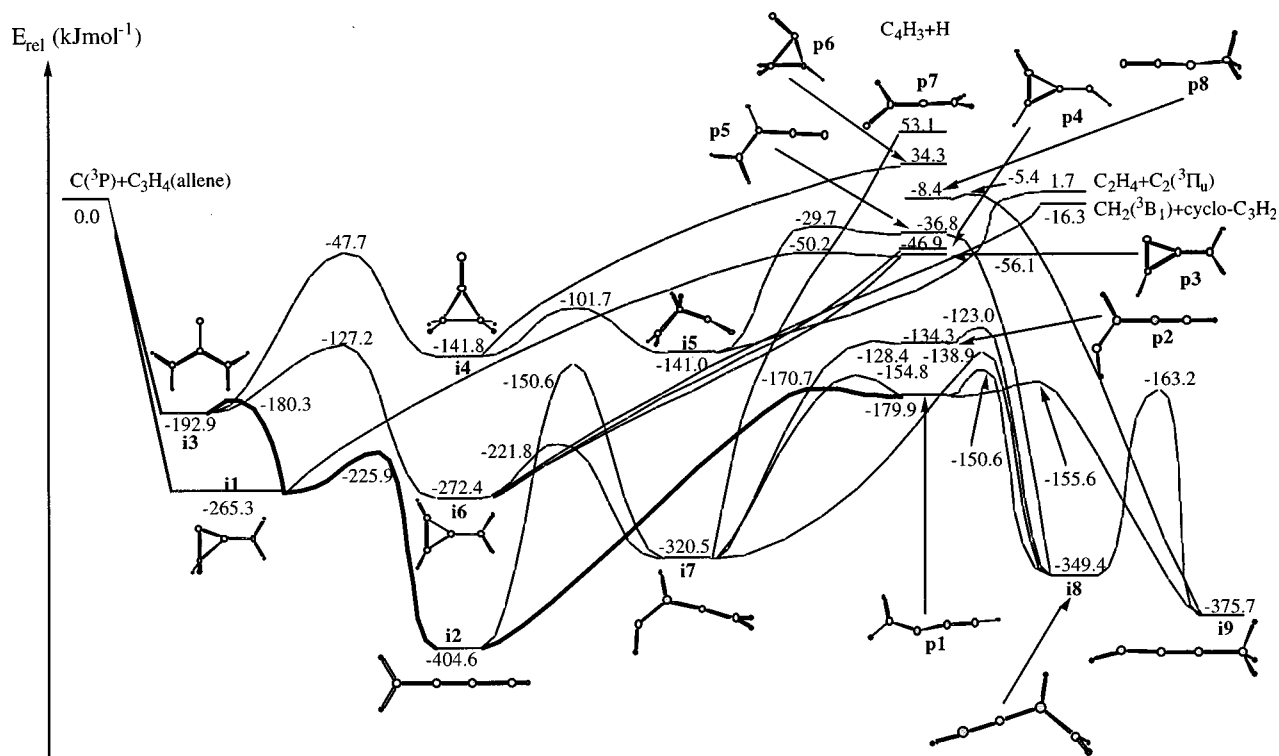


FIG. 9. Schematic representation of the lowest-energy pathways on the triplet C_4H_4 PES and structures of potentially involved collision complexes. Those structures designated with “i” indicate intermediates, those with “p” potential C_4H_3 isomers.

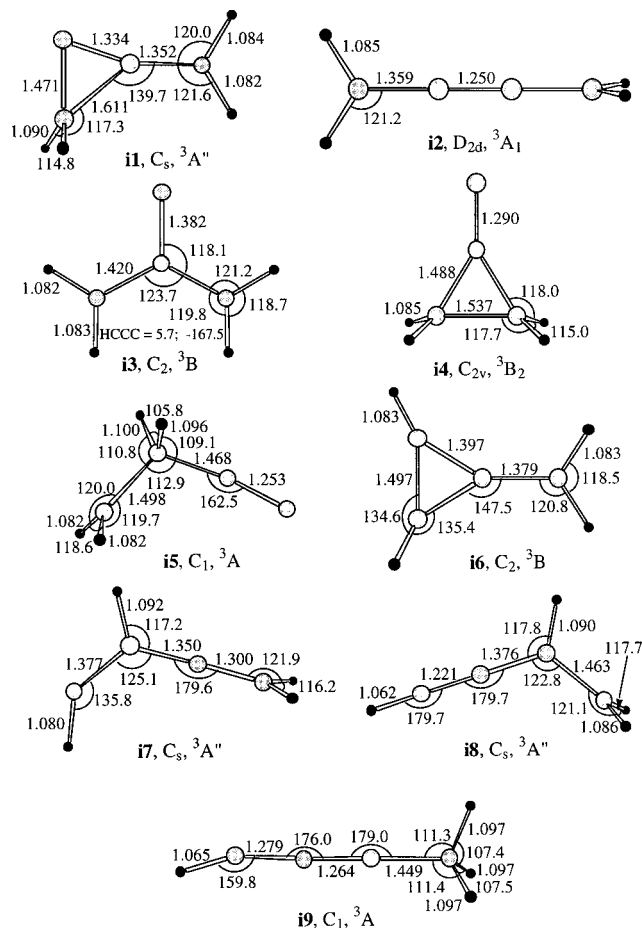


FIG. 10. Structures of potentially involved triplet C_4H_4 collision complexes. Bond lengths are given in Angstroms, bond angles in degrees. Those structures designated with "i" indicate intermediates, those with "p" potential C_4H_3 isomers.

A. The C_4H_4 potential energy surface

1. Addition to the $C=C$ double bond

The *ab initio* calculations reveal that $C(^3P_j)$ can add without entrance barrier to one allenic $C=C$ double bond to form a triplet cyclopropylidene derivative *i1*, Figs. 9–11. This isomer is stabilized by $265.3 \text{ kJ mol}^{-1}$ with respect to the reactants, belongs to the C_s point group, and has a $^3A''$ electronic wave function. (*i1*) ring opens with a barrier of 39.4 kJ mol^{-1} to triplet butatriene (*i2*; $D_{2d}; ^3A_1$) which represents the global minimum of the triplet C_4H_4 potential energy surface (PES) and is bound by $404.6 \text{ kJ mol}^{-1}$. In addition, *i1* could lose an H-atom to form the C_4H_3 isomer *p3* ($C_s, ^2A'$). The exit barrier of this process is only 5.9 kJ mol^{-1} above the products. *i2* either emits an H-atom to form the *n*- C_4H_3 isomer *p1* ($C_s, ^2A'$) through a productlike transition state located only 9.2 kJ mol^{-1} above *n*- C_4H_3+H or depicts a [1,2]-H migration to form C_4H_4 isomer *i7* ($C_s, ^3A''$). The barrier for this migration lies below the total available energy of our crossed-beam reactions. *i7* can fragment via C–H bond cleavage to three different C_4H_3 isomers, i.e., *p1*, *p2* ($C_s, ^2A'$), and *p7* ($C_1, ^2A$). The exit barriers of these pathways are 25.1 kJ mol^{-1} , 5.9 kJ mol^{-1} , and 0 kJ mol^{-1} . In addition, *i7* can undergo two successive H-atom migrations to *i8* ($C_s, ^3A''$)

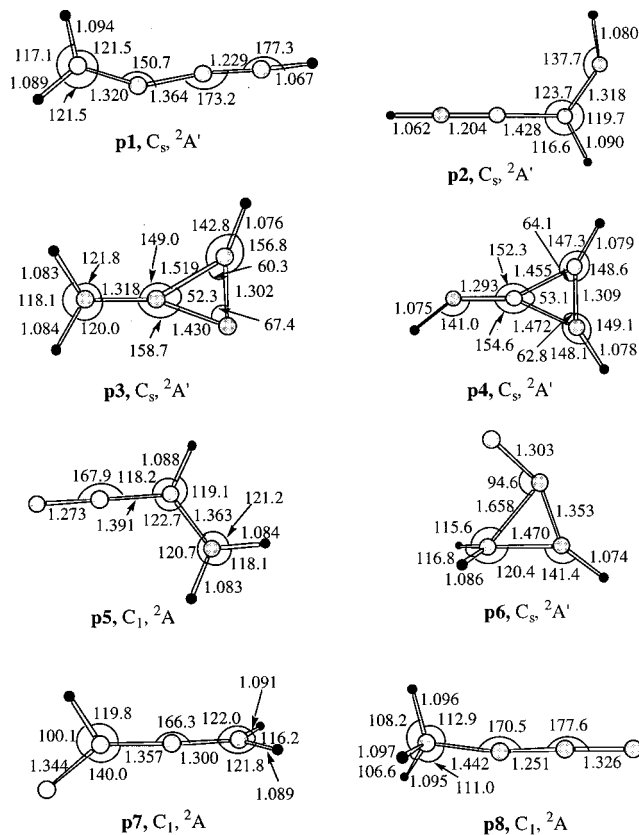


FIG. 11. Structures of doublet C_4H_3 isomers. Bond lengths are given in Angstroms, bond angles in degrees. Those structures designated with "i" indicate intermediates, those with "p" potential C_4H_3 isomers.

and *i9* ($C_1, ^3A$) through barriers of $181.6 \text{ kJ mol}^{-1}$ and $186.2 \text{ kJ mol}^{-1}$. *i8* can fragment through H-atom emission to form *p1* or *p2*, *i9* to *p1* and *p8*. The barrier for fragmentation of *i8* are located 29.3 and 11.3 kJ mol^{-1} above the products, of *i9* to *p1* 24.3 kJ mol^{-1} , and to *p8* 3.0 kJ mol^{-1} . Based on *ab initio* calculations and our relative collision energies we can conclude that reaction to *p7* is too endothermic to occur. Finally, the *ab initio* calculations showed that the transition state of the isomerization of *p1* to *p2* and vice versa is located 46.1 kJ mol^{-1} above the reactants and hence energetically not accessible in our experiments at collision energies of 19.6 and 38.8 kJ mol^{-1} .

2. Addition to the central allenic carbon atom

$C(^3P_j)$ could attack the central carbon atom of the allene molecule without entrance barrier to form a triplet C_4H_4 diradical *i3* ($C_2, ^3B$) which is energetically favored by $192.9 \text{ kJ mol}^{-1}$ compared to $C(^3P_j)+H_2CCCH_2$. Here, each terminal allene carbon atom holds one unpaired electron. The fate of *i3* can be three-fold. First, the barrier to ring closure yielding *i1* is only 12.6 kJ mol^{-1} . Second, an H-atom migration combined with a ring closure can form C_4H_4 isomer *i6* through a tight transition state 65.7 kJ mol^{-1} above *i3*. *i6* is stabilized by $272.4 \text{ kJ mol}^{-1}$ with respect to the reactants, belongs to the C_2 point group, and shows a 3B electronic wave function. C–H bond rupture in *i6* can yield either C_4H_3 isomer *p3* ($C_s, ^2A'$) or *p4* ($C_s, ^2A'$) without exit barrier ex-

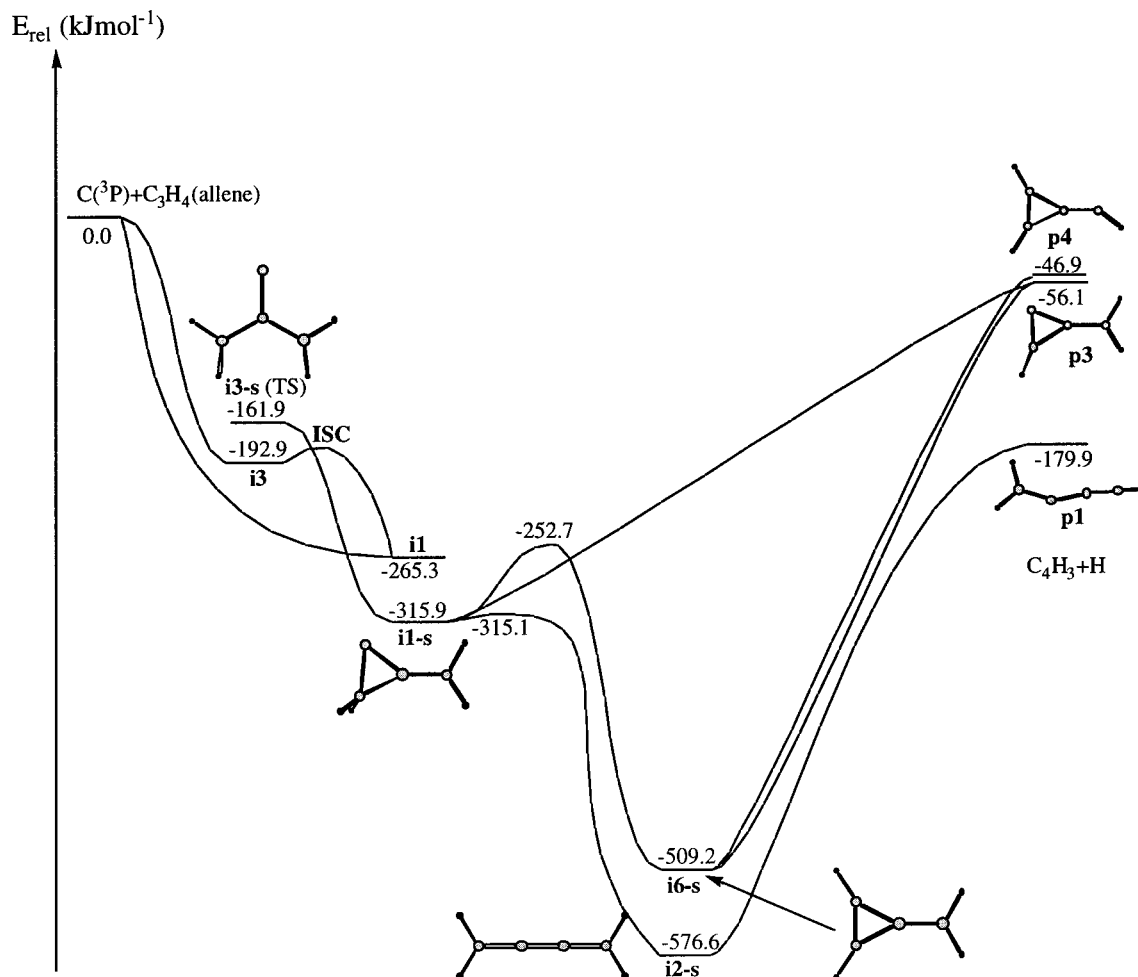


FIG. 12. Schematic representation of the lowest-energy pathways on the singlet C_4H_4 PES and structures of potentially involved collision complexes.

cept the reaction endothermicity. Likewise, $i6$ could ring open through a barrier of 50.6 kJ mol^{-1} to $i7$. Third, $i3$ might show a ring closure to form $i4(C_{2v}, ^3B_2)$ through a barrier of $145.2 \text{ kJ mol}^{-1}$. $i4$ either shows a barrierless C–H bond rupture to yield C_4H_3 isomer $p6(C_s, ^2A')$ or ring opens to triplet C_4H_4 isomer $i5(C_1, ^3A)$, barrier= 40.1 kJ mol^{-1} prior to C–H bond rupture to form C_4H_3 isomer $p5(C_1, ^2A)$, exit barrier= 7.1 kJ mol^{-1} .

3. Insertion into C–H bond

Despite a careful search, no transition states of a $C(^3P_j)$ insertion into the allenic C–H bond could be found. We started the saddle point optimization from the geometries with a CCH three-membered ring suggesting that the C–H bond of allene is broken and two new bonds, C–C and C–H with the attacking carbon atom are formed during the insertion process. This process would lead directly to $i7$. However, the energies of the initial structures are very high. Upon transition state optimization, the C–H bond of allene is restored, the system descends to the vicinity of $i3$ or $i1$, and the optimization does not converge to a saddle point. This indicates that the trajectories directly leading from $C(^3P_j) + H_2CCCH_2$ to $i7$ require high energies

and do not contain a first order hill top. The low-energy pathways from the reactants to $i7$ go through $i3$ and $i6$ or $i1$ and $i2$.

4. Intersystem crossing (ISC)

The triplet C_4H_4 isomer $i3$ fulfils the requirements for a potential intersystem crossing (ISC), cf. Figs. 12 and 13. Here, the two unpaired electrons are placed in p_x and p_z orbitals located on both terminal carbon atoms of the former allene molecule. In this case, orbital angular momentum and spin can be changed simultaneously:²⁵ for the reaction from $i3$ to $i1-s$, this results in a $\alpha \rightarrow \beta$ spin flip and $p_x \rightarrow p_z$ orbital angular momentum change. Thus the overall angular momentum is conserved, and both unpaired electrons are now in the plane containing four carbon atoms, ring closure to singlet C_4H_4 $i1-s$. $i3-s$ is 31.0 kJ mol^{-1} less stable than the triplet isomer. A frequency analysis shows that $i3-s$ is not a local minimum, but a transition state to the singlet C_4H_4 isomer $i1-s$. $i1-s$ belongs to the C_s point group, holds a fully symmetric $^1A'$ electronic wave function, and is $315.9 \text{ kJ mol}^{-1}$ stabilized as compared to the reactants. It either undergoes H-atom migration via a 63.2 kJ mol^{-1} barrier to form $i6-s$ ($C_{2v}, ^1A_1$), or ring opens almost barrierless to singlet butatriene $i2-s$ ($D_{2h}, ^1A_g$), or decomposes to form

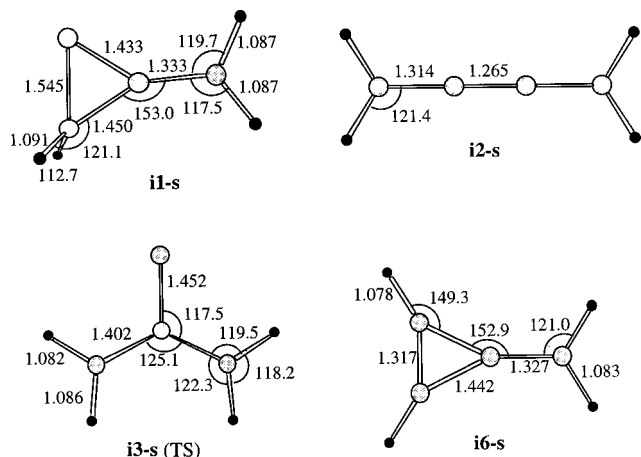


FIG. 13. Structures of potentially involved singlet C₄H₄ collision complexes and transition states (TS). Bond lengths are given in Angstroms, bond angles in degrees. Those structures designated with "i" indicate intermediates.

p3 and atomic hydrogen. *i2-s* represents the global minimum on the singlet C₄H₄ PES and is bound by 576.6 kJ mol⁻¹ with respect to the reactants. Finally, *i6-s* can decompose via C–H cleavage either to *p3* or *p4*, whereas *i2-s*

could fragment to form the most stable C₄H₃ isomer *p1*. All C–H bond ruptures to *p1*, *p3*, and *p3* are barrierless.

B. Reaction pathways on C₄H₄ potential energy surface

In this section, the observed chemical dynamics and energetics are compared to what is expected from our *ab initio* pathways as discussed in the preceding paragraphs. Those channels not compatible with the experimental center-of-mass angular and translational energy distributions are dismissed. This approach ultimately identifies the remaining channel(s) as the only possible one(s). The high-energy cutoff of the $P(E_T)$'s as described in Sec. IV C strongly suggest the formation of the *n*-C₄H₃ isomer *p1* and possibly *i*-C₄H₃ *p2*. Remaining C₄H₃ isomers such as *p3* are at least 123.8 kJ mol⁻¹ less stable than *p1* and are expected to contribute only to a minor amount to the reactive scattering signal.

1. Pathways to *n*-C₄H₃

a. In-plane approach toward the C=C bond. What are the underlying chemical dynamics to yield *n*-C₄H₃? Conserving the C–C–C–C plane as a plane, the singly occupied orbitals of C(³P_{*j*}) could interact in-plane with the π orbital at the carbon–carbon double bond under C_s symmetry on the

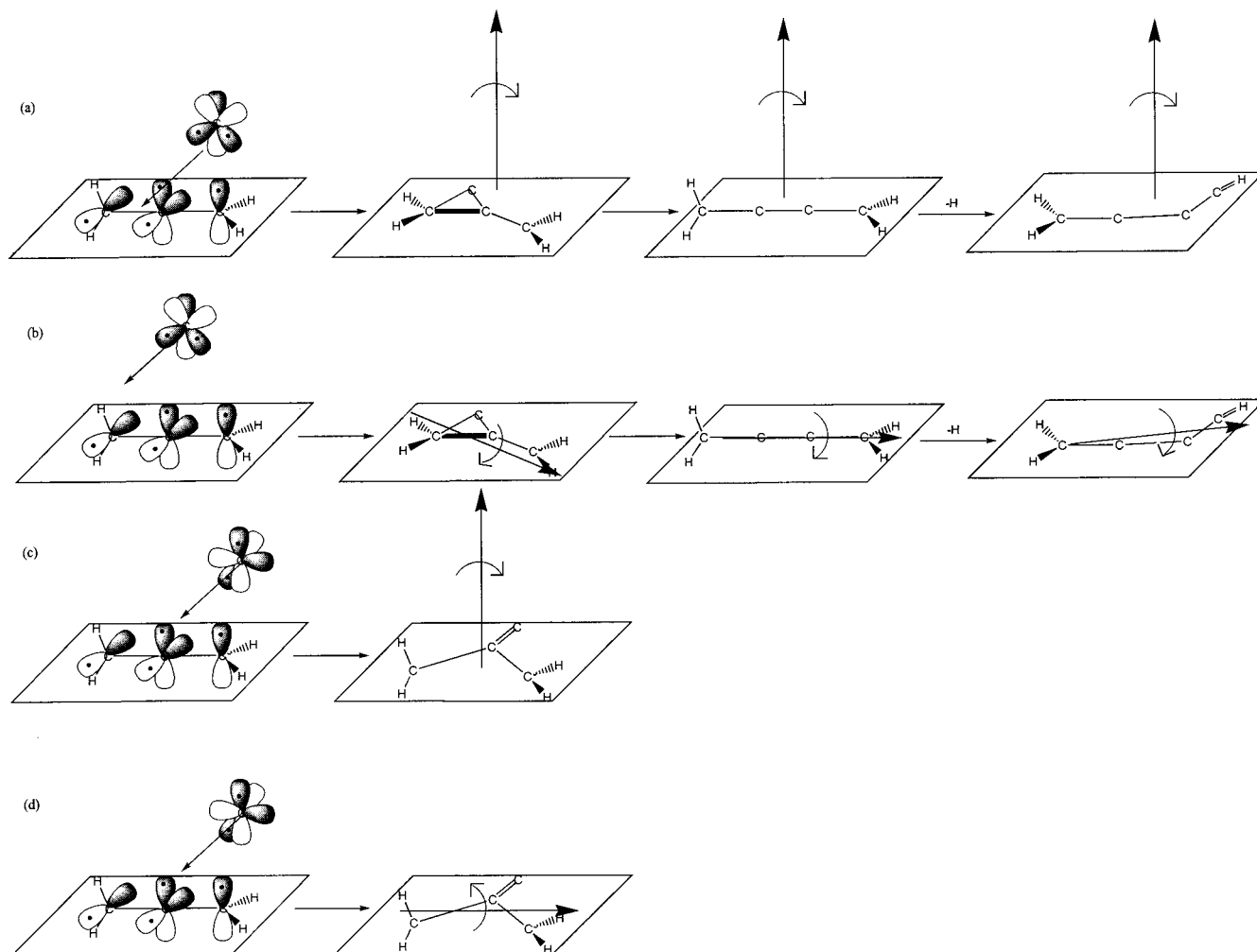


FIG. 14. Approach geometries of C(³P_{*j*}) toward the allene molecule and involved rotations. (a) in-plane approach toward the C=C bond; (b) out-of-plane approach to the C=C bond; (c) in-plane approach toward the central carbon atom.

$^3A''$ surface to form $i1$, cf. Fig. 14(a). This pathway supports a maximum orbital overlap to form two C–C– σ bonds in the cyclopropylidene substructure. Since $L \approx j'$, the four carbon atoms rotate in a plane approximately perpendicular to L around the C -axis of the prolate C_4H_4 isomer $i1$ which has an asymmetry parameter $\kappa = -0.8736$. The consecutive ring opening conserves the rotational axis C of the highly prolate triplet butatriene $i2$, $\kappa = -0.999996$. Since this complex is excited to C -like rotations, the added carbon atom and both H-atoms located at terminal carbon atom are located on opposite sites of the rotation axis as required to explain the forward peaking $T(\theta)$ at higher collision energies. These findings give strong support of the osculating complex model as suggested in Sec. IV D: At lower collision energy, the lifetime of $i2$ is longer than the rotational period around the C axis; with increasing collision energy increases, the lifetime is reduced to less than one rotation period. Based on these results, a symmetric C_4H_4 complex in which H-atoms can be interconverted through a rotation axis to give rise to a symmetric $T(\theta)$ at lower collision energy can be dismissed: first, rotation of $i2$ around the C axis does interconvert any H-atoms. Second, hypothetical A -like rotations of $i2$ around the C_2 axis could interconvert both H-atoms, but these rotations are energetically not accessible. Here, angular momentum conservation requires that $i2$ is excited to $j(i2) = 114\hbar$ at a collision energy of 19.6 kJ mol^{-1} . Using the *ab initio* rotational constants of $i2$ of $A = 4.85151 \text{ cm}^{-1}$ and $B = C = 0.12789 \text{ cm}^{-1}$, and the asymmetric top approximation, about $63000 \text{ kJ mol}^{-1}$ are needed to excite A -like rotations. Considering a maximum available internal energy of $424.8 \text{ kJ mol}^{-1}$, only less than 0.7% of $i2$ populate A rotational states, and most of $i2$ are excited to C -like rotations as deduced above. A final C–H bond rupture in $i2$ yields the $n\text{-}C_4H_3$ isomer, rotating around its C -axis. We like to point out that our proposed chemical dynamics to form $n\text{-}C_4H_3$ through an initial addition to $i1$, followed by ring opening to form $i2$ and a final C–H bond rupture is consistent with large impact parameters leading to the reaction within orbiting limits. This overwhelming contribution of large impact parameters to the capture process up to 3.8 \AA was already mentioned in Secs. IV D and E. Here, our relative cross sections increase as the collision energy drops, strongly indicating no entrance barrier to the reaction. This gains strong support from our *ab initio* calculations since despite a careful search no barrier could be found in the entrance channel to form $i1$. Besides our in-plane approach, out-of-plane approach geometries exciting C -like rotations in $i1$ are supported as well and open larger impact parameters for the reaction.

In addition to $i2$, the complexes $i7$, $i8$, and/or $i9$ can go through H-atom emission to form $p1 + H$ as well. Our experimental data alone cannot identify the decomposing complex, and we employ RRKM calculations to tackle this problem. The rate equations for the title reaction were derived according to Fig. 15 and solved with the rate constants computed by the RRKM theory. As a result, the concentration of each species present in the reaction mechanism was obtained as a function of time. The concentration of the products at $t \rightarrow \infty$ were then taken to calculate the branching ratios.²⁶

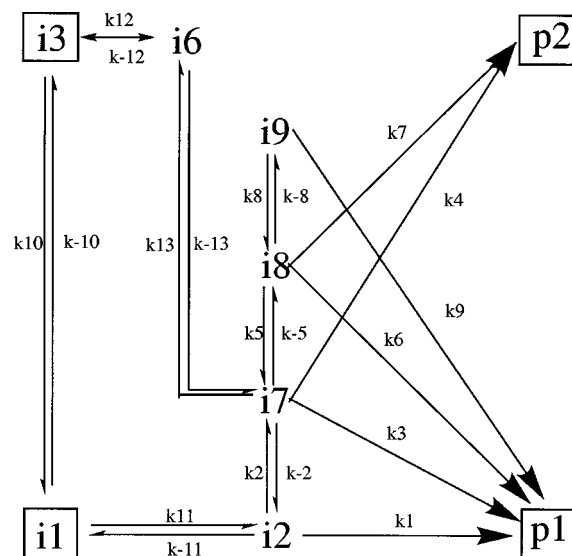


FIG. 15. Diagram showing the reaction pathways included in our RRKM calculations.

Table III shows the calculated rate constants with and without tunneling corrections for each elementary step in Fig. 15, and the additional k_{14} and k_{15} for the reaction $i3 \rightarrow i4$ and $i1 \rightarrow p3$, respectively. The rate equations derived from Fig. 15 were solved for two cases that P is from $i2$, $i7$, $i8$, and $i9$ are distinguishable and nondistinguishable. Our *ab initio* calculations show no entrance barriers for the atomic carbon attack of the allene molecule. Moreover, the RRKM theory can be applied only for unimolecular reactions. Therefore, at the present stage we cannot calculate the branching ratio for the attack of the C=C bond (pathway 1 to $i1$) versus the central carbon atom (pathway 2 to $i1$). To circumvent this problem, the resulting branching ratios for $p1$ and $p2$ were expressed as a function of $i1$ and $i3$ initial concentrations which were not known. The computed branching ratios listed in Tables IV, V, and VI were obtained by plugging in the assumed composition between the initial concentrations of $i1$ and $i3$ in steps of 0.1. At both collision energies, it is evident that more than 96.7% of the $n\text{-}C_4H_3$ isomer is formed through decomposition of $i2$. The results of these calculations indicate that successive H-atom migrations from $i2$ to $i7$, $i8$, and $i9$ play no role in the chemical dynamics of the reaction of atomic carbon with allene molecules.

b. Out-of-plane approach toward the C=C bond. Besides in-plane approach geometries, we have to take out-of-plane attack of $C(^3P_j)$ to the C=C bond conserving C_1 symmetry as well. As evident from Fig. 14(b), these trajectories excite predominantly A -like rotations in Eq. (1) and—after a subsequent ring opening—in $i2$ as well. A final C–H bond fission leads ultimately to $n\text{-}C_4H_3$ isomers in A rotational states. However, detailed energy and angular momentum conservation considerations in the previous section already excluded A -like rotations of $i2$ intermediate as well as $n\text{-}C_4H_3$ product isomer since they cannot be covered energetically. Hence, we conclude that these approach geometries very likely play no contribution in the chemical dynamics of the title reaction.

c. In-plane and out-of-plane approaches toward the cen-

TABLE III. RRKM rate constants in units of s^{-1} as depicted in Fig. 15. The ones computed with tunneling correction are given in parentheses.

	19.6 kJ mol ⁻¹		38.8 kJ mol ⁻¹
k_1	2.91×10^{11}	(2.91×10^{11})	4.94×10^{11}
k_2	8.26×10^9	(9.08×10^9)	1.48×10^{10}
k_{-2}	7.41×10^{10}	(8.15×10^{10})	1.19×10^{11}
k_3	1.75×10^{11}	(1.77×10^{11})	2.84×10^{11}
k_4	2.24×10^{11}	(2.25×10^{11})	4.18×10^{11}
k_5	2.88×10^{10}	(3.09×10^{10})	4.95×10^{10}
k_{-5}	3.28×10^9	(3.51×10^9)	5.83×10^9
k_6	2.88×10^{10}	(2.93×10^{10})	4.96×10^{10}
k_7	3.20×10^9	(3.22×10^9)	6.33×10^9
k_8	6.03×10^{10}	(6.52×10^{10})	9.57×10^{10}
k_{-8}	7.61×10^9	(8.24×10^9)	1.25×10^{10}
k_9	1.14×10^9	(1.15×10^9)	1.95×10^9
k_{10}	1.13×10^{12}	(1.13×10^{12})	1.17×10^{12}
k_{-10}	7.18×10^{11}	(7.20×10^{11})	9.09×10^{11}
k_{11}	1.34×10^{13}	(1.34×10^{13})	1.49×10^{13}
k_{-11}	1.86×10^{10}	(1.87×10^{10})	2.51×10^{10}
k_{12}	5.04×10^{10}	(5.15×10^{10})	6.65×10^{10}
k_{-12}	1.57×10^{10}	(1.61×10^{10})	2.54×10^{10}
k_{13}	4.92×10^{12}	(4.95×10^{12})	5.56×10^{12}
k_{-13}	2.50×10^{11}	(2.51×10^{11})	3.07×10^{11}
k_{14}^a	3.46×10^7	(3.69×10^7)	8.86×10^7
k_{15}^b	1.80×10^9	(1.81×10^9)	6.48×10^9

^a $i3 \rightarrow i4$.^b $i1 \rightarrow p3$.

tral C atom of the allene molecule. The singly occupied p_x and p_z orbitals of the carbon atom could add to the π_x and π_z orbitals of the allene molecule to form $i3$, Fig. 14(c)/(d). This orbital interaction shows a maximum orbital overlap to the central carbon atom and forms a C–C– σ and C–C– π bond via interaction of p_x with π_x and p_z with π_z orbitals, respectively. These trajectories results in $i3$ rotating either around the C [all four carbon atoms rotate in one plane; case (c)] or A axis [case (d)]. As outlined above, $i3$ can rearrange to $i1$, whose fate is described in Sec. VB 1 a, or to $i6$. Hence, trajectories leading to A excitations can be ruled out since the reaction sequence $i3 \rightarrow i1 \rightarrow i2$ would lead to $i2$ intermediates which must rotate around their A axis as well. However, this rotational excitation is energetically not accessible. Therefore, only approach geometries giving rise to C excitations could form $i2$ through $i3 \rightarrow i1 \rightarrow i2$. Since the barrier for $i3 \rightarrow i1$ is only 12.6 kJ mol⁻¹ compared to 65.7 kJ mol⁻¹

TABLE IV. Branching ratio to form n -C₄H₃ isomers from intermediates $i2$, $i7$, $i8$, and $i9$ at a collision energy of 19.6 kJ mol⁻¹. ($i1, i3$) means the fraction of $i1$ intermediate to $i3$ intermediates. See text for details.

($i1, i3$)	$i2 \rightarrow p1$	$i7 \rightarrow p1$	$i8 \rightarrow p1$	$i9 \rightarrow p1$
(0, 1)	164.38	4.38	0.48	0.13
(0.1, 0.9)	155.44	3.89	0.43	0.12
(0.2, 0.8)	146.42	3.42	0.38	0.10
(0.3, 0.7)	137.33	2.99	0.33	0.09
(0.4, 0.8)	128.17	2.58	0.28	0.08
(0.5, 0.5)	118.94	2.21	0.24	0.07
(0.6, 0.4)	109.63	1.86	0.20	0.06
(0.7, 0.3)	100.26	1.55	0.17	0.05
(0.8, 0.2)	90.81	1.26	0.14	0.04
(0.9, 0.1)	81.29	1.00	0.11	0.03
(1, 0)	71.70	0.77	0.09	0.02

TABLE V. Branching ratio to form n -C₄H₃ isomers from intermediates $i2$, $i7$, $i8$, and $i9$ at a collision energy of 38.8 kJ mol⁻¹. ($i1, i3$) means the fraction of $i1$ intermediate to $i3$ intermediates. See text for details.

($i1, i3$)	$i2 \rightarrow p1$	$i7 \rightarrow p1$	$i8 \rightarrow p1$	$i9 \rightarrow p1$
(0, 1)	152.25	4.54	0.53	0.14
(0.1, 0.9)	143.57	4.00	0.46	0.13
(0.2, 0.8)	134.81	3.49	0.40	0.11
(0.3, 0.7)	125.95	3.02	0.35	0.09
(0.4, 0.8)	117.00	2.58	0.30	0.08
(0.5, 0.5)	107.96	2.18	0.25	0.07
(0.6, 0.4)	98.83	1.81	0.21	0.06
(0.7, 0.3)	89.62	1.47	0.17	0.05
(0.8, 0.2)	80.30	1.17	0.14	0.04
(0.9, 0.1)	70.90	0.91	0.10	0.03
(1, 0)	61.41	0.67	0.08	0.02

and 145.2 kJ mol⁻¹ for reactions $i3 \rightarrow i6$ and $i3 \rightarrow i4$, formation of $i1$ should dominate these processes due to the lowest barrier. This is in strong agreement with our results since $i4$ would yield only the C₄H₃ isomers $p5$ and $p6$. $i6$ could rearrange to $i7$ which loses an H-atom to form n -C₄H₃. However, angular momentum conservation dictates that $i7$ is excited to C-like rotations, but the incorporated carbon atom and the leaving H-atom are located on the same site of the rotation axis and cannot account for the forward peaked center-of-mass angular distribution at higher collision energy. Hence, the reaction sequence $i3 \rightarrow i6 \rightarrow i7 \rightarrow p1$ can be excluded from the discussion as well. Based on our experimental data alone, we cannot quantify the contribution of the $i3 \rightarrow i1$ sequence to yield $p1$. As discussed above, however, large impact parameters should dominate the chemical dynamics. The attack of C(³P_j) to the central allenic C atom involves only small impact parameters less than 0.65 Å. Therefore we conclude that this microchannel should contribute to a minor extent compared to addition of atomic carbon to the C=C bond of allene. Since our data suggest the reaction proceeds within orbiting limits, the contribution of trajectories with a smaller impact parameter—and hence the contribution of microchannel $i3 \rightarrow i1$ —should decrease as the collision energy rises.

TABLE VI. Branching ratio of n - to i -C₄H₃ isomers. The ratios with tunneling correction are in parentheses. ($i1, i3$) means the fraction of $i1$ intermediate to $i3$ intermediates. See text for details.

($i1, i3$)	19.6 kJ mol ⁻¹	38.8 kJ mol ⁻¹
(0, 1)	169 (152)	157
(0.1, 0.9)	160 (144)	148
(0.2, 0.8)	150 (135)	139
(0.3, 0.7)	141 (127)	129
(0.4, 0.8)	131 (119)	120
(0.5, 0.5)	121 (110)	110
(0.6, 0.4)	112 (101)	101
(0.7, 0.3)	102 (93)	91
(0.8, 0.2)	92 (85)	82
(0.9, 0.1)	82 (76)	72
(1, 0)	73 (68)	62

2. Pathways to *i*-C₄H₃

The center-of-mass translational energy distributions cannot rule out minor contributions of the *i*-C₄H₃ isomer *p*2. Based on our *ab initio* calculations, *p*2 can be synthesized through C–H bond rupture of C₄H₄ intermediate *i*7. *i*7 itself is either formed through ring opening of *i*6 or H-atom shift in *i*2. As already discussed above, trajectories with large impact parameters should dominate the chemical dynamics. Therefore the reaction sequence *i*3→*i*6→*i*7 should be only of minor importance, and *i*7 is likely to be formed predominantly through H-atom migration from *i*2 rotating around its *C* axis, cf. Sec. V B 1. Alternatively, decomposition of *i*8 can lead to *p*2+H as well. Based on our experimental data, we cannot quantify the contribution of the *i*-versus *n*-C₄H₃ isomer. As evident from Table VI, the computed ratios of the *n*-C₄H₃ isomer is more than 98.4%, and *n*-C₄H₃ dominates the chemical dynamics of the title reaction.

C. Possible contributions from the singlet C₄H₄ potential energy surface

As discussed in Sec. V A 4, the C₄H₄ isomer *i*3 fulfills requirements for ISC to form eventually *i*1-*s* on the singlet C₄H₄ surface. The shape of the center-of-mass translational energy distribution helps to unravel the contribution of the singlet surface. Both *P*(*E*_T)'s peak at about 30–50 kJ mol⁻¹ indicating a tight exit transition state from the decomposing C₄H₄ intermediate to the products. However, our *ab initio* calculations depict no exit barrier to form *p*1, *p*3, or *p*4 +H. Hence, our *P*(*E*_T)'s are expected to peak at 0 kJ mol⁻¹—in strong contrast to our findings. In addition, a minor barrier of only 0.8 kJ mol⁻¹ favors a ring opening of *i*1-*s* to *i*2-*s*. *A*-, *B*-, as well as *C*-like rotations of *i*2-*s* are expected to show a symmetric center-of-mass angular distributions at both lower and higher collision energies since each rotation interconverts the hydrogen atoms, and H departs with equal probability into *θ* and *θ*-*π* to result in a *T*(*θ*) symmetric around *π*/2. Hence, only *i*1-*s* and *i*6-*s* remain. A detailed analysis of the rotational axes and taking into account that the leaving H and incorporated C atom must be placed on different sides of the rotational axis shows that only *i*1-*s* excited to *A* to form *p*3, and *i*6-*s* excited to *B*-like rotations to yield *p*4 can fulfill this requirement. If we consider energy conservation and calculate the energy necessary to excite *A*-like rotations in *i*1-*s* employing the rigid rotor approximation, we find that these rotations are only accessible for 5% of the intermediates. In addition, formation of *p*3 and/or *p*4 expects to show a high-energy cutoffs in the *P*(*E*_T)'s between 60 and 80 kJ mol⁻¹, in strong disagreement with our data. Based on these arguments, we conclude that if ISC provides reactive scattering signal of the title reaction, this contribution is likely small.

D. Lifetime of the decomposing complex

The rotational period of the decomposing C₄H₄ isomers *i*2 acts as a clock in the molecular beam experiment and can be utilized to estimate the lifetime *τ* of the fragmenting com-

plex at a relative collision energy of 38.8 kJ mol⁻¹. The oscillating model relates the intensity ratio of *T*(*θ*) at both poles to *τ* via Eq. (10);

$$I(180^\circ)/I(0^\circ) = \exp\left(-\frac{t_{\text{rot}}}{2\tau}\right), \quad (10)$$

where *t*_{rot} represents the rotational period with:

$$t_{\text{rot}} = 2\pi I_i / L_{\text{max}}. \quad (11)$$

*I*_{*i*} represents the moment of inertia of the complex rotating around the *i*-axis, and *L*_{max} the maximum orbital angular momentum. Using our *ab initio* geometries we yield rotational periods of the complexes and plug in all data in Eq. (10). We calculate lifetimes of *i*2 rotating around the *A*, *B*, and *C* axes to *τ*(*A*)=0.017 ps, and *τ*(*B*)=*τ*(*C*)=0.66 ps. Accounting for the uncertainties in the center-of-mass angular distribution, these data are within 10%–20%. As evident, the magnitude of *τ* depends strongly on the rotation axis, i.e., *B*, *C*, vs *A*. Since reactions with a collision times ≪0.1 ps follow direct scattering dynamics and expect to show almost zero intensity at large angles of the center-of-mass angular distribution, the *T*(*θ*) at our higher collision energy is expected to be strongly forward peaked, if the complex rotated around the *A* axis. This is clearly not observed in the experiment. Hence a rotation about the *A* axis of all complexes can be excluded as already suggested in the previous paragraphs, and the end-over-end rotation dominates.

E. Comparison with the reaction C(³*P*_{*j*}) + CH₃CCH

The reaction between ground state carbon atoms, C(³*P*_{*j*}), and methylacetylene, CH₃CCH (*X*¹*A*₁), was studied recently at averaged collision energies of 20.4 and 33.2 kJ mol⁻¹ using the crossed molecular beams technique.⁵ The reaction dynamics indicate that the carbon atom attacks the *π*-orbitals of the methylacetylene molecule via a loose, reactantlike transition state located at the centrifugal barrier. The initially formed triplet 1-methylpropendiyldene complex rotates in a plane almost perpendicular to the total angular momentum vector around the *B*/*C*-axes and undergoes [2,3]-hydrogen migration to triplet 1-methylpropargylene. Within 1–2 ps, the complex decomposes via C–H bond cleavage to *n*-C₄H₃ and atomic hydrogen.

Compared to the reaction of C(³*P*_{*j*}) with H₂CCCH₂, data at higher collision energies of both C₃H₄ isomers show identical laboratory angular distribution and TOF spectra. Likewise, the center-of-mass angular as well as translational distributions are identical within the error limits. Finally, the fragmentation pattern and intensity of the integrated TOFs at *m/e*=51, 50, and 49 are the same, i.e., 0.5(*m/e*=51):1.0(*m/e*=50):0.25(*m/e*=49). However, at lower collision energies, the lab and center-of-mass distributions differ significantly. In addition, the fragmentation ratios of at *m/e*=51, 50, and 49 of the C(³*P*_{*j*}) + H₂CCCH₂ reaction are identical to those obtained at higher collision energy within the error limits. This pattern is expected, since at both collision energies the *n*-C₄H₃ isomer is formed. But data of the reaction of atomic carbon with methylacetylene yield (*m/e*=51):(*m/e*=50):(*m/e*=49)=0.3:1.0:0.5. This sug-

gests that at lower collision, the reaction of carbon with methylacetylene and allene forms distinct isomers. Based on the high-energy cutoff of the center-of-mass translational energy distribution of the reaction of carbon with allene, the authors postulated the formation of a higher-energy isomer possibly a cyclic isomer, however, without an explicit identification.²⁷ The postulation of a higher-energy isomer gains additional support if we consider the averaged fraction of energy channeling into the translational degrees of freedom. At collision energies between 19.6 and 45.0 kJ mol⁻¹, our data reveal that the reaction of atomic carbon with all unsaturated hydrocarbons containing three carbon atoms such as propylene C₃H₆, allene H₂CCCH₂, and methylacetylene CH₃CCH except the latter at lower collision energies brings 30%–35% of the total available energy into kinetic energy of the product—almost independent on the collision energy and the reaction product. High level *ab initio* calculations on the C/CH₃CCH together with variational RRKM calculations are underway to resolve the outstanding question of the C₄H₃ isomer formed at lower collision energy.

F. Comparison with the reaction O(³P_j) + H₂CCCH₂

The reaction of O(³P_j) with allene was studied recently at a collision energy of 33.5 kJ mol⁻¹.²⁸ Three reaction channels were found. First, trajectories with small impact parameters are governed by an attack of O(³P_j) to the central allenic carbon atom form a triplet diradical which undergoes intersystem crossing to the singlet surface. The entrance barrier to this center addition is found to be less than 33.5 kJ mol⁻¹. A ring closure leads to cyclopropanone which fragments via an open CO–CH₂–CH₂ diradical through a tight exit transition state to CO and C₂H₄. This reaction proceeds through a long-lived complex and is exothermic by

500.3 kJ mol⁻¹. In the reaction of C(³P_j) with allene, however, the similar channel to C₂(¹Σ_g⁺) + C₂H₄ is closed despite its exothermicity of 8 kJ mol⁻¹. As discussed in Sec. VB, addition to the central carbon atom leads to *i*8, followed by ISC to form *i*3-*s*. The singlet form of *i*3 represents not a local minimum, but a transition state. Hence, a singlet CC–CH₂–CH₂ diradical analogous to CO–CH₂–CH₂ cannot be formed. On the triplet surface, reaction to C₂(³Π_u) + C₂H₄ is endothermic by only 3.2 kJ mol⁻¹. Reaction must involve the addition complexes *i*3, *i*4, and *i*5. However, *i*3 prefers ring closure to *i*1 compared to *i*4. In Table III, the RRKM rate constants *k*₁₄, *k*₁₂, and *k*₁₀ calculations show ratios of 3.3 × 10⁻⁵:4.5 × 10⁻²:1.9 and 7.6 × 10⁻⁵:5.7 × 10⁻²:1.0 at our lower and higher collision energies for the reaction sequences *i*3 → *i*4, *i*3 → *i*6, and *i*3 → *i*1, strongly supporting that *i*3 → *i*1 dominates.

The second and third channels in the reaction of O(³P_j) with allene are governed by an addition to the terminal carbon atom which either fragments directly through C–H bond rupture to form H₂C=C–COH (channel 2) or undergoes H-atom migration to yield triplet acrolein. The authors suggest a consecutive ISC to singlet acrolein followed by a C–C bond rupture to yield C₂H₃ and HCO. The differences in the chemical dynamics to the C(³P_j) + allene reaction are the direct consequence of the potential energy surface. Here, an open triplet diradical as an addition product of C(³P_j) to the terminal carbon atom holds no local minimum on the triplet C₄H₄ PES as shown in our *ab initio* calculations, but undergoes ring closure followed by a ring opening to triplet butatriene. Likewise, our title reaction has no entrance barrier, whereas the analogous O(³P_j) reaction has an entrance barrier of at least 33.5 kJ mol⁻¹. Hence, the latter reaction does not proceed within orbiting limits, and a larger fraction of smaller impact parameters is expected to lead to reaction,

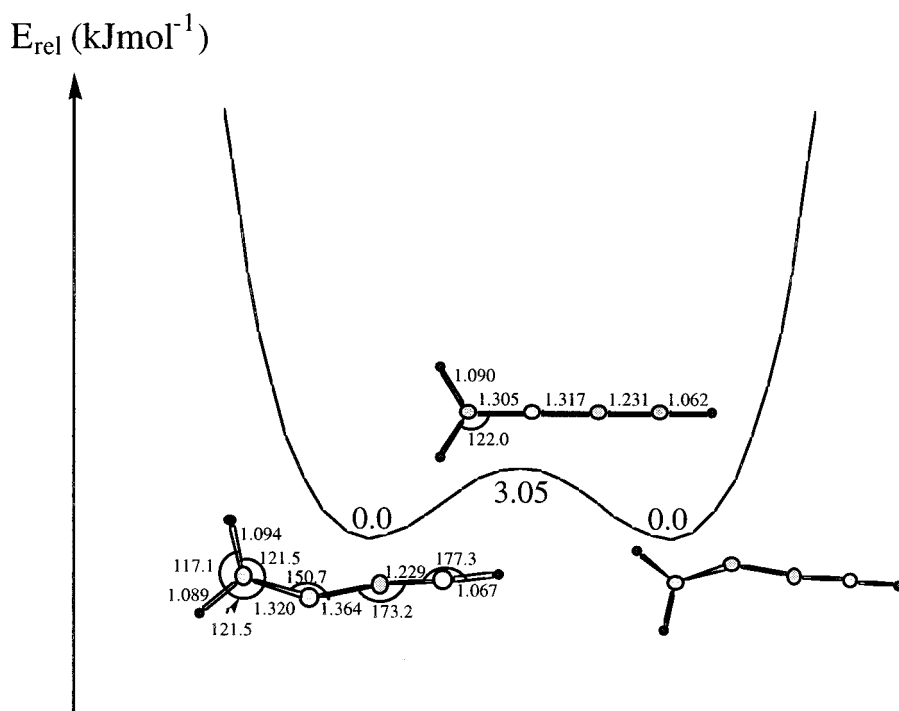


FIG. 16. Double potential energy well of the *n*-C₄H₃ isomer and its linear transition state. Bond lengths are given in Angstroms, bond angles in degrees.

such as those approaches where the oxygen atom attacks the central carbon atom of the allene molecule.

VI. IMPLICATIONS TO INTERSTELLAR CHEMISTRY AND COMBUSTION PROCESSES

The identification of the n -C₄H₃ isomer under single collision conditions is of importance to chemical reaction networks modeling the temporal development of chemistry in molecular clouds, hot molecular cores, outflow of carbon stars, and hydrocarbon-rich planetary atmospheres. Hitherto, information on distinct structural isomers as reaction products were lacking and hence could not be included in these schemes. The present study underlines this importance, since C(³P_{*j*}) + CH₃CCH leads to a second, probably cyclic C₄H₃ isomer at lower, but to n -C₄H₃ at higher collision energies, whereas C(³P_{*j*}) + H₂CCCH₂ forms n -C₄H₃ at lower as well as higher collision energies. In addition, the barrierless nature of the reactions of atomic carbon with allene and methylacetylene demonstrates explicitly that these processes are of potential importance in even coldest interstellar clouds such as TMC-1 with typical translational temperatures of 10 K. Methylacetylene, CH₃CCH, has been widely observed toward dark, molecular clouds such as OMC-1 and TMC-1 in high fractional abundances between $(4-6) \times 10^{-9} \text{ cm}^{-3}$ through microwave spectroscopy.²⁹ A second C₃H₄ isomer, allene (H₂CCCH₂), holds no permanent electric dipole moment and hence shows no rotational spectrum. Although H₂CCCH₂ should be detectable via infrared spectroscopy in the circumstellar shell of, e.g., the carbon star IRC+10216, this isomer has escaped any astronomical identification so far. Despite this failure, the allene isomer is strongly expected to be present.³⁰

Moreover, terrestrial based microwave spectra of C₄H₃ radicals should be recorded and transitions sought in interstellar environments. Here, especially the situation of the n -C₄H₃ is extremely interesting: the ground state is a bent structure *p*1, cf. Fig. 16, whereas the linear butatrienyl structure represents a transition state between two bent states, located only 255 cm⁻¹ above the n -C₄H₃, cf. Fig. 16. Since coldest molecular clouds have averaged translational temperatures of about 10 K—about 7 cm⁻¹— n -C₄H₃ must be bent. The transition state is energetically not accessible. In hotter interstellar environments such as hot molecular cores with averaged translational temperatures of 200–300 K—about 140–210 cm⁻¹—C₄H₃ radicals populating translational energies in the long tail of the Maxwell–Boltzmann distribution could overcome the barrier, cf. Fig. 16, and these radical should be quasi-linear. Radicals with lower kinetic energies must be bent. Therefore, the microwave spectrum of the n -C₄H₃ radical depends strongly on the temperature of the interstellar environments. Vice versa, recording these microwave spectra could serve as a probe to sample the temperature in these environments. Likewise, the assignment of the n -C₄H₃ radical under our single collision conditions as well as via trapping experiments in oxygen-rich hydrocarbon flames supports inclusion of C₄H₃ hydrocarbon radicals even in oxidative hydrocarbon flames.

VII. CONCLUSIONS

The reaction between ground state carbon atoms, C(³P_{*j*}), and allene, H₂CCCH₂, was studied at averaged collision energies of 19.6 and 38.8 kJ mol⁻¹ using the crossed molecular beam technique. The carbon atom attacks the π orbitals of the allene molecule barrierless via a loose, reactantlike transition state located at the centrifugal barrier. The initially formed cyclopropylidene derivative rotates in a plane almost perpendicular to the total angular momentum vector **J** around its *C* axis and undergoes ring opening to triplet butatriene. Within 0.6 ps, the complex decomposes via hydrogen emission to the n -C₄H₃ isomer through a tight exit transition state. As the collision energy increases, the approach geometries with smaller impact parameter very likely show in enhanced contribution leading to a barrierless attack of C(³P_{*j*}) to the central carbon atom in the allene molecule. The explicit identification of the n -C₄H₃ radical under single collision represents a further example of a carbon–hydrogen exchange in reactions of ground state carbon atoms with unsaturated hydrocarbons. This channel opens a versatile pathway to synthesize extremely reactive hydrocarbon radicals relevant to combustion processes, interstellar chemistry, and chemical modification of hydrocarbon-rich atmospheres of Jupiter, Saturn, Titan, as well as Triton.

ACKNOWLEDGMENTS

R.I.K. is indebted the Deutsche Forschungsgemeinschaft for a *Habilitation* fellowship (IIC1-Ka1081/3-1). This work was supported by Academia Sinica, Taiwan, the National Science Council of R.O.C., and partly by the U.S. Department of Energy under Contract No. DE-AC03-76SF00098. A partial support from the Petroleum Research Fund of R.O.C. is also appreciated.

- ¹R. D. Kern, K. Xie, and H. Chen, *Combust. Sci. Technol.* **85**, 77 (1992); R. D. Smith, *Combust. Flame* **35**, 179 (1979); I. R. Slagle and D. Gutman, *Proc. 23rd Symp. Int. Combust. Chemistry*, 875 (1988); L. R. Thorne, M. C. Branch, D. W. Chandler, R. J. Kee, and J. Miller, *Proc. 21st Symp. Int. Combust. Chemistry*, 965 (1986).
- ²Symposium on Titan, ESA-SP 338, ESTEC, Noordwijk (1992).
- ³E. Herbst, H. H. Lee, D. A. Howe, and T. J. Millar, *Mon. Not. R. Astron. Soc.* **268**, 335 (1994).
- ⁴P. R. Westmoreland *et al.*, *J. Phys. Chem.* **93**, 8171 (1989); S. P. Walsh, *J. Chem. Phys.* **103**, 8544 (1995).
- ⁵R. I. Kaiser, D. Stranges, Y. T. Lee, and A. G. Suits, *J. Chem. Phys.* **105**, 8721 (1996).
- ⁶C. Ochsenfeld, R. I. Kaiser, A. G. Suits, Y. T. Lee, and M. Head-Gordon, *J. Chem. Phys.* **106**, 4141 (1997); R. I. Kaiser, C. Ochsenfeld, M. Head-Gordon, Y. T. Lee, and A. G. Suits, *Science* **274**, 1508 (1996); R. I. Kaiser, Y. T. Lee, and A. G. Suits, *J. Chem. Phys.* **105**, 8705 (1996); R. I. Kaiser, D. Stranges, Y. T. Lee, and A. G. Suits, *ibid.* **105**, 8721 (1996); R. I. Kaiser, D. Stranges, H. M. Bevssek, Y. T. Lee, and A. G. Suits, *ibid.* **106**, 4945 (1997); R. I. Kaiser, W. Sun, A. G. Suits, and Y. T. Lee, *ibid.* **107**, 8713 (1997).
- ⁷Y. T. Lee, J. D. McDonald, P. R. LeBreton, and D. R. Herschbach, *Rev. Sci. Instrum.* **40**, 1402 (1969).
- ⁸R. I. Kaiser and A. G. Suits, *Rev. Sci. Instrum.* **66**, 5405–5410 (1995).
- ⁹G. O. Brink, *Rev. Sci. Instrum.* **37**, 857 (1966).
- ¹⁰M. S. Weis, Ph. D. thesis, University of California, Berkeley (1986); M. Vernon, Thesis, University of California, Berkeley (1981).
- ¹¹A. D. Becke, *J. Chem. Phys.* **97**, 9173 (1992).
- ¹²C. Lee, W. Yang, and R. G. Parr, *Phys. Rev. B* **37**, 785 (1988).
- ¹³R. Krishnan, M. Frisch, and J. A. Pople, *J. Chem. Phys.* **72**, 4244 (1988).
- ¹⁴G. D. Purvis and R. J. Bartlett, *J. Chem. Phys.* **76**, 1910 (1982).

- ¹⁵A. M. Mebel, K. Morokuma, and M. C. Lin, *J. Chem. Phys.* **103**, 7414 (1995).
- ¹⁶L. A. Curtiss, K. Raghavachari, and J. A. Pople, *J. Chem. Phys.* **98**, 1293 (1993).
- ¹⁷M. J. Frisch, G. W. Trucks, H. B. Schlegel, P. M. W. Gill, B. G. Johnson, M. A. Robb, J. R. Cheeseman, T. Keith, G. A. Petersson, J. A. Montgomery, K. Raghavachari, M. A. Al-Laham, V. G. Zakrzewski, J. V. Ortiz, J. B. Foresman, J. Cioslowski, B. B. Stefanov, A. Nanayakkara, M. Challacombe, C. Y. Peng, P. Y. Ayala, W. Chen, M. W. Wong, J. L. Andres, E. S. Replogle, R. Gomperts, R. L. Martin, D. J. Fox, J. S. Binkley, D. J. Defrees, J. Baker, J. P. Stewart, M. Head-Gordon, C. Gonzalez, and J. A. Pople, GAUSSIAN 94, Revision D.4 (Gaussian, Inc., Pittsburgh, PA, 1995).
- ¹⁸MOLPRO is a package of *ab initio* programs written by H.-J. Werner and P. J. Knowles, with contributions from J. Almlöf, R. D. Amos, M. J. O. Deegan, S. T. Elbert, C. Hampel, W. Meyer, K. Peterson, R. Pitzer, A. J. Stone, P. R. Taylor, and R. Lindh.
- ¹⁹J. F. Stanton, J. Gauss, J. D. Watts, W. J. Lauderdale and R. J. Bartlett, ACES-II, University of Florida, USA.
- ²⁰A. Mebel *et al.*, *J. Chem. Phys.* (in preparation).
- ²¹H. Eyring, S. H. Lin, and S. M. Lin, *Basis Chemical Kinetics* (Wiley, New York, 1980).
- ²²W. H. Miller, *J. Am. Chem. Soc.* **101**, 6810 (1979).
- ²³W. B. Miller, S. A. Safron, and D. R. Herschbach, *Discuss. Faraday Soc.* **44**, 108 (1967); W. B. Miller, Ph.D. thesis, Harvard University, Cambridge (1969).
- ²⁴D. C. Clary, N. Haider, D. Husain, and M. Kabir, *Astrophys. J.* **422**, 416 (1994).
- ²⁵N. J. Turro, *Modern Molecular Photochemistry* (University Science Books, Milla Valley, 1991); Y. N. Chiu and S. F. A. Abidi, *J. Phys. Chem.* **86**, 3288 (1982).
- ²⁶A. H. H. Chang, A. M. Mebel, X. M. Yang, S. H. Lin, and Y. T. Lee, *J. Chem. Phys.* **109**, 2748 (1998).
- ²⁷R. I. Kaiser, C. Ochsenfeld, D. Stranges, M. Head-Gordon, and Y. T. Lee, *Faraday Discuss.* **109**, 183 (1998).
- ²⁸A. M. Schmoltner *et al.*, *J. Chem. Phys.* **99**, 1644 (1993).
- ²⁹E. C. Sutton, R. Peng, W. C. Danchi, P. A. Jaminet, G. Sandell, and A. P. G. Russel, *Astrophys. J. Suppl.* **97**, 455 (1995); F. Combes, G. Wlodarczak, P. Encrenaz, and C. Laurent, *Astron. Astrophys.* **253**, L29 (1992).
- ³⁰T. J. Millar, P. R. A. Farquhar, and K. Willacy, *Astron. Astrophys., Suppl. Ser.* **121**, 139 (1997).